Key Points:
- Alfvén-cyclotron instability maximum growth rate scales linearly with hot proton temperature anisotropy
- Alfvén-cyclotron instability field energy scales linearly with hot proton temperature anisotropy
- Instability growth and saturation scalings can be written as concise closed-form expressions

Correspondence to:
S. P. Gary,
pgary@lanl.gov

Scalings for the Alfvén-cyclotron instability: Linear dispersion theory and hybrid particle-in-cell simulations

S. Peter Gary[1] , Xiangrong Fu[2] , Misa M. Cowee[3] , Dan Winske[3] , and Kaijun Liu[4]

[1]Space Science Institute, Boulder, Colorado, USA, [2]New Mexico Consortium, Los Alamos, New Mexico, USA, [3]Los Alamos National Laboratory, Los Alamos, New Mexico, USA, [4]Department of Physics, Auburn University, Auburn, Alabama, USA

Abstract The Alfvén-cyclotron instability is driven by an ion temperature anisotropy such that $T_\perp/T_\| > 1$ where $\perp$ and $\|$ denote directions perpendicular and parallel to a uniform background magnetic field $\mathbf{B}_o$, respectively. The computations presented here consider a model of a magnetized, homogeneous, collisionless plasma. Two representations of the proton velocity distribution are considered: a single bi-Maxwellian and a magnetospheric-like configuration of two components, a more dense, relatively cool, isotropic component and a less dense, relatively hot, bi-Maxwellian component which drives the instability. Only wave propagation parallel to $\mathbf{B}_o$ is considered. Using numerical solutions of the full kinetic linear dispersion equation, concise analytic expressions for the scaling of the dimensionless maximum instability growth rate and the corresponding dimensionless real frequency are derived as functions of three dimensionless variables: the hot proton temperature anisotropy, the relative hot proton density, and the hot proton $\beta_\|$. Furthermore, using one-dimensional hybrid particle-in-cell simulations of this same instability, a third relation for the scaling of the maximum amplitude of the dimensionless fluctuating magnetic field energy density is derived.

1. Introduction

The Alfvén-cyclotron instability in collisionless plasmas is driven by an ion temperature anisotropy of the type $T_\perp/T_\| > 1$ where $\perp$ and $\|$ denote directions perpendicular and parallel to a uniform background magnetic field $\mathbf{B}_o$, respectively [*Gary*, 1993]. This free energy excites enhanced fluctuating magnetic and electric fields at real frequencies (ω_r) and growth rates (γ) less than Ω_p, the proton cyclotron frequency, maximum growth rates (denoted by γ_m) at $\mathbf{k} \times \mathbf{B}_o = 0$ and wave numbers satisfying $kc/\omega_p \leq 1$ where ω_p denotes the proton plasma frequency. This instability is observed to arise in many different space plasmas including the solar wind [*Gary et al.*, 2016 and references therein], the terrestrial magnetosheath [*Anderson et al.*, 1994 and references therein], and the terrestrial magnetosphere [*Anderson et al.*, 1992; *Gary et al.*, 1995; *Fraser and Nguyen*, 2001; *Meredith et al.*, 2003; *Min et al.*, 2012; *Zhang et al.*, 2014], where the resulting enhanced fluctuations are often termed "electromagnetic ion cyclotron" (EMIC) waves.

If large-scale magnetospheric processes drive sufficiently large proton anisotropies, the consequent growth of the Alfvén-cyclotron instability leads to enhanced field fluctuations that scatter those protons, reducing those anisotropies so as to stabilize the instability and to impose an upper bound on the anisotropies. Using hybrid PIC (particle-in-cell) simulations in which ions are represented as an ensemble of superparticles but the electrons are described more simply in terms of a fluid model to describe this proton-driven instability, *Gary et al.* [1997] showed that this upper bound can be expressed in the form

$$T_{\perp p}/T_{\| p} - 1 = S_p/\beta_{\| p}{}^{\alpha p}$$

where $0.4 \leq \alpha_p \leq 0.5$, $S_p < 1$, subscript p represents protons and subscript e represents electrons. Here we define $\beta_{\| j} \equiv 8\pi n_j T_{\| j}/B_o{}^2$ where j represents the jth plasma component. It is also convenient to use, at times, a β defined in terms of the total electron density, that is, $\widetilde{\beta}_{\| j} \equiv 8\pi n_e T_{\| j}/B_o{}^2$. These fluctuations also scatter relativistic electrons causing the detrapping of such particles from the terrestrial magnetosphere [*Liu et al.*, 2010 and citations therein]. Although the plasma physics of these processes is understood in a qualitative sense, quantitative representations of this physics have not yet been formulated due to their strongly nonlinear character and to the large number of physical variables needed to describe space plasmas in environments such as the magnetosphere.

Currently, the most favored approach to the modeling of magnetospheric dynamics involves computations of the large-scale, slowly varying behavior of the plasma [*Jordanova et al.*, 2014 and citations therein]. Computational limitations prevent such models from including small-scale, high-frequency wave processes. Various approaches have been proposed to include small-scale physics into large-scale models of the magnetosphere but, to our knowledge, each of these approaches has made substantial simplifications with respect to either or both of the nonlinear physics or the broad range of plasma parameters.

A general approach to understanding the consequences of ion-driven instability growth in magnetospheric plasmas is to use kinetic linear dispersion theory in conjunction with hybrid PIC simulations obtain analytic expressions for the scaling properties of enhanced fluctuations. Kinetic linear dispersion theory can yield concise analytic expressions for the maximum growth rate of the Alfvén-cyclotron instability. Then a large number of nonlinear hybrid PIC simulations [*Fu et al.*, 2016] may be used to yield further analytic expressions relating maximum growth rates with fluctuating field amplitudes, the proton temperature anisotropies, and $\beta_{\|p}$ at instability saturation. Under the assumption that the time scales for instability growth and saturation are faster than the time rates of change of large-scale magnetospheric processes, these analytic expressions can then be inserted into large-scale models of the magnetosphere to provide simple but accurate expressions for the physical consequences of Alfvén-cyclotron instability growth.

The first step toward implementing such a self-consistent procedure for incorporating the nonlinear physics and the extensive range of plasma parameters for EMIC fluctuations in the inner terrestrial magnetosphere is to obtain concise scaling relations for the properties of growing modes such as the Alfvén-cyclotron instability. *Fu et al.* [2016] used both linear dispersion theory and hybrid PIC simulations to compute such relations between the maximum linear growth rate and the saturation wave amplitude of this instability. Here we use the same tools to consider the maximum growth rate, the real frequency at maximum growth, and the fluctuating magnetic field energy density at saturation of the Alfvén-cyclotron instability as dependent variables and derive their scaling relations as functions of three independent variables: the hot proton temperature anisotropy, the relative density of the hot proton component, and $\beta_{\|h}$.

In section 2 we derive analytic forms of the scaling relations for the Alfven-cyclotron instability for the relatively simple model in which there is a single, hot, anisotropic proton component. In section 3 we consider the more realistic, but more complex, case of two proton constituents, a relatively dense, relatively cool, isotropic component and a relatively tenuous, relatively hot, anisotropic component. In section 4 we use one-dimensional hybrid PIC simulations of this same instability to derive a relation for the scaling of the maximum amplitude of the fluctuating magnetic field energy density. Section 5 is a summary and conclusion. Throughout this manuscript the plasma frequency of the jth component is denoted as ω_j, and the cyclotron frequency of the jth component is represented by Ω_j.

2. Kinetic Linear Dispersion Theory: Hot Protons Only

Solutions of the kinetic linear dispersion equation for the Alfvén-cyclotron instability driven by a proton temperature anisotropy yield maximum growth rates at propagation parallel or antiparallel to $\mathbf{B}_o$. Thus, under the assumption that both protons and electrons are represented by bi-Maxwellian velocity distributions, the kinetic dispersion equation for electromagnetic waves and instabilities at $\mathbf{k} \times \mathbf{B}_o = 0$ in homogeneous, collisionless, magnetized plasmas, for example, *Gary* [1993, equation (7.1.6)] can then be used to determine the scalings of the dependent dimensionless variables γ_m/Ω_p and the corresponding dimensionless real frequency ω_m/Ω_p as functions of the independent dimensionless variables $\beta_{\|p}$ and $T_{\perp p}/T_{\|p}$. For typical magnetospheric parameters the maximum growth rate of the Alfvén-cyclotron instability is independent of v_A/c and T_e/T_p so that the scaling relations we derive in this section are well described as functions only of the proton temperature anisotropy and $\beta_{\|p}$. We use $v_A/c = 4.67 \times 10^{-4}$ and $T_e/T_p = 1.0$ for the linear theory results of this section.

Gary [1993, equation (7.1.8)] suggests that, for sufficiently large proton temperature anisotropies, the maximum growth rate of the Alfvén-cyclotron instability is a linear function of $T_{\perp p}/T_{\|p}$. More specifically, *Bortnik et al.* [2011, Figure 5], *Fu et al.* [2016, Figure 3], and sample calculations not displayed here show that the
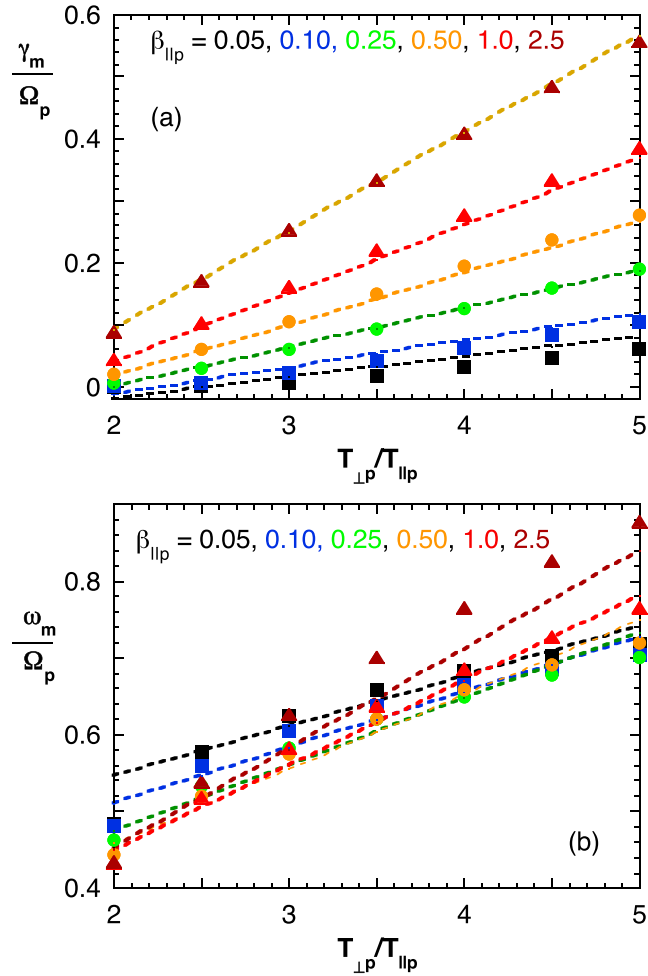
Figure 1. This figure represents results for the case in which the protons are modeled as a single bi-Maxwellian velocity distribution. The symbols indicate solutions to the kinetic linear dispersion equation for the Alfvén-cyclotron instability at $\mathbf{k} \times \mathbf{B}_o = 0$ as a function of the proton temperature anisotropy, and the dashed lines represent equation (1) with equations (2a) and (2b) and equation (3) with equations (4a) and (4b). Black corresponds to $\beta_{\|p} = 0.05$, blue to $\beta_{\|p} = 0.10$, green to $\beta_{\|p} = 0.25$, orange to $\beta_{\|p} = 0.50$, red to $\beta_{\|p} = 1.0$, and dark red to $\beta_{\|p} = 2.5$. (a) The maximum instability growth rate and (b) the real frequency corresponding to the maximum growth rate.

maximum growth rate of this mode is approximately proportional to $T_{\perp p}/T_{\|p}$ for values of this parameter greater than 2 and less than 5. So we assume the functional form

$$\gamma_m/\Omega_p = g_1 + g_2 \left(T_{\perp p}/T_{\|p} \right) \tag{1}$$

where g_1 and g_2 are functions only of $\beta_{\|p}$. Figure 1a shows that, for the $\beta_{\|p}$ values used here and the given proton anisotropies, γ_m/Ω_p at constant values of $\beta_{\|p}$ indeed satisfies equations of the form of (1). If we then fit this equation to the points of Figure 1a, we obtain

$$g_1 \cong - 0.18\beta_{\|p}^{0.25} \tag{2a}$$

and

$$g_2 \cong 0.11\beta_{\|p}^{0.40} \tag{2b}$$

which provides a closed-form expression for the maximum linear growth rate of this instability on the parametric domain $2 \leq T_{\perp p}/T_{\|p} \leq 5$ and $0.25 \leq \beta_{\|p} \leq 2.5$. The dashed lines of Figure 1a are equation (1) with equations (2a) and (2b).

We further hypothesize that the real frequency corresponding to γ_m/Ω_p is also a linear function of the proton temperature anisotropy so that by analogy with equation (1), we assume for $2 \leq T_{\perp p}/T_{\|p} \leq 5$

$$\omega_m/\Omega_p = f_1 + f_2\left(T_{\perp p}/T_{\|p}\right) \tag{3}$$

Figure 1b plots ω_m/Ω_p computed from the kinetic linear dispersion theory as a function of this temperature anisotropy for six different values of $\beta_{\|p}$. This figure clearly demonstrates that, for the given range of the hot proton anisotropy, the dispersion equation yields ω_m/Ω_p values which satisfy equation (3). Fitting these six curves to equation (3) gives approximate scalings for the two fitting parameters:

$$f_1 \cong 0.23\beta_{\|p}^{-0.20} \tag{4a}$$

and

$$f_2 \cong 0.11\beta_{\|p}^{0.18} \tag{4b}$$

The dashed lines in Figure 1b are equation (3) with equations (4a) and (4b).

The quality of these approximate fits to the exact results obtained from the kinetic linear dispersion equation are discussed in Appendix A. Table A1 shows that the fits to ω_m/Ω_p are generally good for all values of $\beta_{\|p}$ considered here, but that the quality of fits to γ_m/Ω_p is good only for relatively large values of $\beta_{\|h}$. The poor fits are apparently associated with the relatively small values of maximum growth rates at low $\beta_{\|p}$.

## 3. Kinetic Linear Dispersion Theory: Hot Protons Plus Cool Protons

To consider conditions more appropriate for the magnetosphere, this section describes a linear dispersion analysis of the Alfvén-cyclotron instability in a model plasma with two distinct proton contributions, a relatively cool, isotropic, more dense component (denoted by subscript c) and a relatively hot, anisotropic, less dense component (denoted by subscript h) with $n_c + n_h = n_e$, $T_e = T_c$ and $T_{\|c} \ll T_{\|h}$. As in *Fu et al.* [2016] we use kinetic linear dispersion theory as described in *Gary* [1993, section 7.1.2] with the electron and cool proton components represented as Maxwellian velocity distributions and the hot proton component represented as a bi-Maxwellian. Again, as in *Fu et al.* [2016], we assume that the maximum instability growth rate is at $\mathbf{k} \times \mathbf{B}_o = 0$ and we compute γ_m/Ω_p and the corresponding ω_m/Ω_p of this instability which here is driven by $T_{\perp h}/T_{\|h} > 1$. As in section 2 and in *Fu et al.* [2016], we find that, for a specified range of parametric variations, the maximum growth rate of the instability as well as the corresponding real frequency are approximately linear functions of the hot proton temperature anisotropy. We then derive approximate analytic expressions for these quantities as functions of three dimensionless variables, $T_{\perp h}/T_{\|h}$, $\beta_{\|h}$, and the relative hot component density n_h/n_e. Here we consider the range $2 \leq T_{\perp h}/T_{\|h} \leq 5$, and $n_h/n_e \ll 1$, as well as the order-of-magnitude range $0.10 \leq \beta_{\|h} \leq 1.0$ which includes the $0.10 \leq \beta_{\|h} \leq 0.25$ values corresponding to the EMIC magnetospheric observations of *Zhang et al.* [2014]. Throughout this section our calculations assume $T_{\|h} = 3000\,T_{\|c}$; sample calculations at different values of $T_{\|h}/T_{\|c} \gg 1$ show no significant changes in γ_m/Ω_p indicating that, for the parameters considered here, the cool protons are noncyclotron resonant with this instability. We use $v_A/c = 4.67 \times 10^{-4}$ and $T_e/T_c = 1.0$ for the linear theory results of this section.

Our first step here was to calculate γ_m/Ω_p and ω_m/Ω_p as functions of $T_{\perp h}/T_{\|h}$ with $\beta_{\|h}$ and n_h/n_e held constant, with the results shown in Figure 2. Figure 2a shows that there is an approximate linear relationship between γ_m/Ω_p and $T_{\perp h}/T_{\|h}$; this also follows from *Gary* [1993, equation (7.1.8)] (Note the missing minus sign in the exponential factor of this equation.) because the cool proton component term vanishes in the limit of zero $T_{\|c}$ (See also *Bortnik et al.* [2011, Figure 5] and *Fu et al.* [2016, Figure 3]). Thus, as in equation (1), we assume for

$$\gamma_m/\Omega_p = g_1 + g_2\left(T_{\perp h}/T_{\|h}\right) \tag{5}$$

and the resulting values of the fitting parameters g_1 and g_2 are as given in Table 1. Using the numbers of this table, various attempts at fitting parameters as functions of $\beta_{\|h}$ and the dimensionless hot proton density suggest the trial functions

$$g_1 = k_1(n_h/n_e)^{\alpha 1}\beta_{\|h}^{\alpha 11} \tag{6a}$$
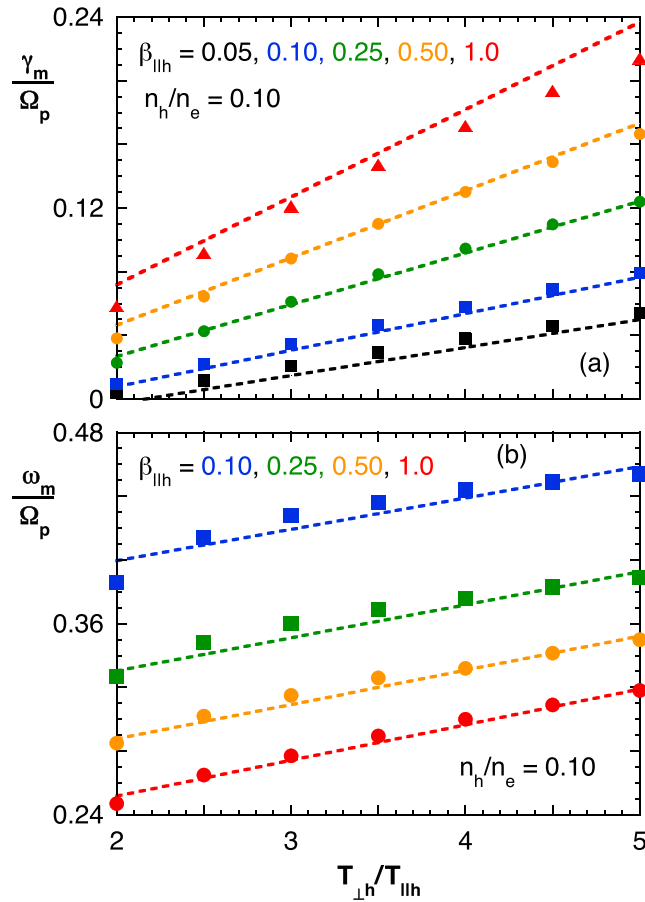
Figure 2. This figure, as well as all subsequent figures, represents results for the case in which the protons are modeled as the sum of cool Maxwellian and hot bi-Maxwellian velocity distributions. The symbols indicate solutions to the kinetic linear dispersion equation for the Alfvén-cyclotron instability at $\mathbf{k} \times \mathbf{B}_o = 0$ as a function of the proton temperature anisotropy at $n_h/n_e = 0.10$ and $\beta_{\|p} = 0.05$ (black points), $\beta_{\|p} = 0.10$ (blue points), $\beta_{\|p} = 0.25$ (green points), $\beta_{\|p} = 0.50$ (orange points), and $\beta_{\|p} = 1.0$ (red points). (a) The maximum instability growth rate where the dashed line represents equation (5) with equations (6a), (6b), and (7) and the colors as stated in the preceding sentence. (b) The real frequency corresponding to the maximum growth rate where the dashed line represents equation (8) with equations (9a), (9b), and (10) and the colors as stated above.

and

$$g_2 = k_2(n_h/n_e)^{\alpha 2}\beta_{\|h}{}^{\alpha 22} \tag{6b}$$

Figure 3 shows the maximum growth rate of this instability as a function of n_h/n_e with the other two dimensionless parameters held to fixed values. Figure 3 demonstrates that, when the maximum growth rate of this instability is computed using the parameters stated here and using a kinetic dispersion equation like *Gary* [1993, equation (7.1.6)] the maximum growth rate is not proportional to n_h, as claimed by *Bortnik et al.*

Table 1. The Fitting Parameters g_1 and g_2 of Equation (5) as Obtained From Solutions of the Linear Dispersion Equation for the Maximum Growth Rate of the Alfvén-Cyclotron Instability for the Parameters $\beta_{\|h}$ and n_h/n_e as Given

g_1	$\beta_{\|h} = 0.10$	$\beta_{\|h} = 0.25$	$\beta_{\|h} = 0.50$	$\beta_{\|h} = 1.0$
$n_h/n_e = 0.05$	−0.0251	−0.0295	−0.0306	−0.0275
$n_h/n_e = 0.10$	−0.0360	−0.0416	−0.0422	−0.0378
$n_h/n_e = 0.20$	−0.0506	−0.0592	−0.0602	−0.0548
g_2	$\beta_{\|h} = 0.10$	$\beta_{\|h} = 0.25$	$\beta_{\|h} = 0.50$	$\beta_{\|h} = 1.0$
$n_h/n_e = 0.05$	0.0180	0.0261	0.0332	0.0403
$n_h/n_e = 0.10$	0.0233	0.0337	0.0425	0.0515
$n_h/n_e = 0.20$	0.0292	0.0425	0.0537	0.0650
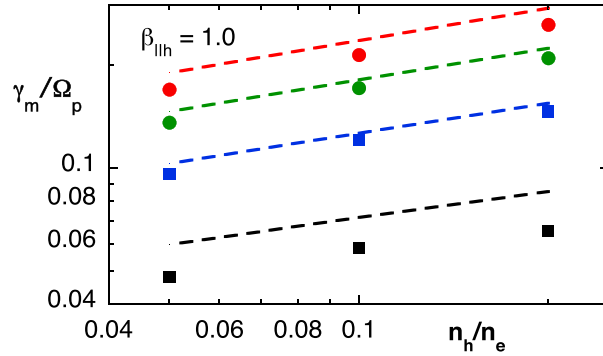
Figure 3. The maximum linear growth rate of the Alfvén-cyclotron instability from the kinetic linear dispersion equation for electromagnetic fluctuations at $\mathbf{k} \times \mathbf{B}_o = 0$ as a function of the dimensionless hot proton density at $\beta_{\|h} = 1.0$ as well as $T_{\perp h}/T_{\|h} = 2.0$ (black points), 3.0 (blue points), 4.0 (green points), and 5.0 (red points). The dashed lines represent equation (5) with equations (6a), (6b), and (7) with the colors corresponding to the hot proton temperature anisotropies stated in the preceding sentence.

[2011]. Rather γ_m/Ω_p is a weaker function of the dimensionless hot proton density, scaling approximately as $(n_h/n_e)^{0.6}$. We believe that our result is the more appropriate conclusion. This is because the dispersion equation of *Gary* [1993] is exact in the linear approximation, and the usual analytic approximation for the linear growth rate, as, for example, in *Gary* [1993, equation (7.1.8)] shows that γ_m/Ω_p is not only an explicit function of n_h/n_e but also an implicit function of the hot proton component relative density through the presence of terms containing the real frequency ω_r.

Then, further fits of the linear theory results to the forms of equations (6a) and (6b) on the ranges $0.10 \leq \beta_{\|h} \leq 1.00$ and $0.05 \leq n_h/n_e \leq 0.20$ yield the following results:

$$
\begin{aligned}
k_1 &\cong - \ 0.12 \\
k_2 &\cong 0.12 \\
\alpha_1 &\cong 0.50 \\
\alpha_2 &\cong 0.34 \\
\alpha_{11} &\cong 0 \\
\alpha_{22} &\cong 0.38
\end{aligned}
\tag{7}
$$

Figure 2b shows that the real frequency corresponding to the maximum growth rate is also a monotonically increasing function of the hot proton temperature anisotropy. By analogy with equation (3) we assume

$$
\omega_m/\Omega_p = f_1 + f_2\left(T_{\perp h}/T_{\|h}\right)
\tag{8}
$$
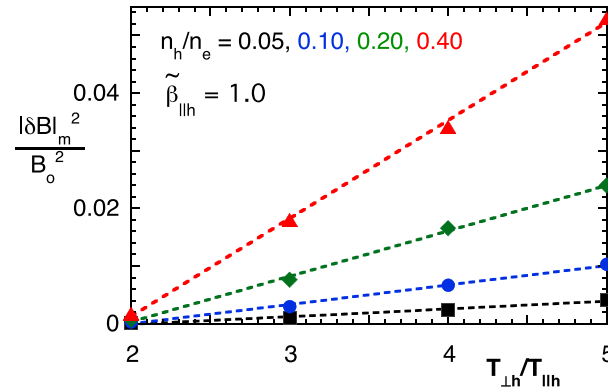
and, by analogy with equations (6a) and (6b),

$$
f_1 = \kappa_1 (n_h/n_e)^{\alpha 1} \beta_{\|h}^{\ \alpha 11}
\tag{9a}
$$

and

$$
f_2 = \kappa_2 (n_h/n_e)^{\alpha 2} \beta_{\|h}^{\ \alpha 22}
\tag{9b}
$$

Then, further fits of the linear theory results to the forms of equations (9a) and (9b) on the ranges $0.10 \leq \beta_{\|h} \leq 1.00$ and $0.05 \leq n_h/n_e \leq 0.20$ yield the following:

$$
\begin{aligned}
\kappa_1 &\cong 0.36 \\
\kappa_2 &\cong 0.074 \\
a_1 &\cong 0.24 \\
a_2 &\cong 0.52 \\
a_{11} &\cong - \ 0.24 \\
a_{22} &\cong 0.054
\end{aligned}
\tag{10}
$$

Figure 4. The maximum dimensionless fluctuating magnetic field energy density of the Alfvén-cyclotron instability from hybrid PIC simulations at $\mathbf{k} \times \mathbf{B}_o = 0$ as a function of the hot proton temperature anisotropy with $\tilde{\beta}_{\|h} = 1.0$. Here the color black corresponds to $n_h/n_e = \beta_{\|h} = 0.05$, blue represents $n_b/n_e = \beta_{\|h} = 0.10$, green stands for $n_b/n_e = \beta_{\|h} = 0.20$, and red means $n_b/n_e = \beta_{\|h} = 0.40$. The individual points represent results from various simulations, and the dashed lines represent equation (11) with fitting parameters ε_1 and ε_2 as given in Table 2.

The dashed lines in Figure 2b are equation (8) with equations (9a), (9b), and (10). The quality of these fits compared to the exact linear dispersion results are again discussed in Appendix A. Table A2 shows that the fits to ω_m/Ω_p are generally good for all values of $\beta_{\|h}$ considered in Figure 2b, but that the quality of fits to γ_m/Ω_p is good only for relatively large values of $\beta_{\|h}$. Once again, the poor fits are associated with the relatively small values of maximum growth rates.

4. Hybrid PIC Simulations: Hot Protons Plus Cool Protons

Gary et al. [1997] showed that scaling relations for the Alfvén-cyclotron instability can be derived for properties at maximum growth rate (using kinetic linear dispersion theory) as well as the maximum value of the fluctuating magnetic field energy density (using nonlinear hybrid particle-in-cell simulations). More recently, *Min et al.* [2016] used full PIC simulations of the Alfvén-cyclotron instability driven by a proton ring velocity distribution to demonstrate that both the maximum growth rate and the saturation levels of the magnetic fluctuation energy density increase monotonically with increasing ion temperature anisotropy. Here, as in *Fu et al.* [2016], we use the one-dimensional Los Alamos hybrid PIC code [*Winske and Omidi*, 1993] to simulate this instability in a homogeneous, magnetized, collisionless plasma model using the same proton velocity distribution described in section 3: a dense, cool, isotropic proton component and a tenuous, hot, anisotropic proton component. The simulation parameters are the same as those stated in *Fu et al.* [2016, Table 2]: there are 256 cells along $\mathbf{B}_o$, the cell size is $1.0\, c/\omega_p$, the time step is $0.05/\Omega_p$, and the number of superparticles per cell per species is 12,000. Using these simulation results, we here derive an analytic expression for the scaling of the maximum fluctuating magnetic field energy density in terms of the same three dimensionless parameters considered in section 3, that is, $T_{\perp h}/T_{\|h}$, $\beta_{\|h}$, and n_h/n_e.

The initial values of the parameters used in this ensemble of simulations are as follows: $\omega_e/\Omega_e = 5$; $\tilde{\beta}_{\|h} = 0.3$, 1.0, 3.0, and 10.0; $n_h/n_e = 0.05$, 0.10, 0.20, and 0.40; and $T_{\perp h}/T_{\|h} = 2.0$, 3.0, 4.0, and 5.0. The consequences of these simulations are similar to the results of earlier one-dimensional hybrid PIC simulations of the Alfvén-cyclotron instability in a plasma of two proton components [*Gary et al.*, 1994, 1995]: the fluctuating magnetic field energy densities reach saturation at $\Omega_p t \sim 200$, the temperature anisotropy of the hot protons is considerably reduced, and the temperature anisotropy of the cool proton component is driven to $T_{\perp c}/T_{\|c} \gg 1$.

Following the format of Figures 1 and 2 above, Figure 4 presents the maximum fluctuating field energy density, $\varepsilon_m \equiv |\delta\mathbf{B}|_m^2/B_o^2$, as a function of the hot proton temperature anisotropy from the $\tilde{\beta}_{\|h} = 1.0$ simulations of this ensemble. The figure shows that, for the range of $2 \le T_{\perp h}/T_{\|h} \le 5$ the maximum fluctuating magnetic field energy density is not only a monotonic function of the hot proton temperature anisotropy but is reasonably well fit as a linear function of that parameter. The same result obtains for the $\tilde{\beta}_{\|h} = 3.0$ and 10.0 simulations of this ensemble. So by analogy with equations (1) and (3), we assume over $2 \le T_{\perp h}/T_{\|h} \le 5$

Table 2. The Fitting Parameters ε_1 and ε_2 of Equation (11) as Obtained From Saturation Values of the Magnetic Fluctuation Energy Densities From Hybrid PIC Simulations of the Alfvén-Cyclotron Instability for the Parameters $\widetilde{\beta}_{\parallel h}$ and n_h/n_e as Given

ε_1	$\widetilde{\beta}_{\parallel h} = 1.0$	$\widetilde{\beta}_{\parallel h} = 3.0$	$\widetilde{\beta}_{\parallel h} = 10.0$
$n_h/n_e = 0.05$	−0.00279	−0.00739	−0.0187
$n_h/n_e = 0.10$	−0.00675	−0.0169	−0.0531
$n_h/n_e = 0.20$	−0.0154	−0.0392	−0.158
$n_h/n_e = 0.40$	−0.0327	−0.0896	−0.284
ε_2	$\widetilde{\beta}_{\parallel h} = 1.0$	$\widetilde{\beta}_{\parallel h} = 3.0$	$\widetilde{\beta}_{\parallel h} = 10.0$
$n_h/n_e = 0.05$	0.00134	0.00427	0.0126
$n_h/n_e = 0.10$	0.00337	0.00992	0.0328
$n_h/n_e = 0.20$	0.00788	0.0231	0.0916
$n_h/n_e = 0.40$	0.0170	0.0522	0.181

$$|\delta \mathbf{B}|_m^2/B_o^2 = \varepsilon_1 + \varepsilon_2\left(T_{\perp h}/T_{\parallel h}\right) \tag{11}$$

where the fitting parameters ε_1 and ε_2 are functions only of $\widetilde{\beta}_{\parallel h}$ and n_h/n_e. The resulting values of the fitting parameters are given in Table 2.

Trial fits at constant values of the dimensionless temperature ratios show that ε_1 and ε_2 are relatively independent of n_h/n_e, so we assume the fitting functions to be

$$\varepsilon_1 = c_1 \beta_{\parallel h}{}^{\eta_{11}} \tag{12a}$$

and

$$\varepsilon_2 = c_2 \beta_{\parallel h}{}^{\eta_{22}} \tag{12b}$$

Using the values of ε_1 and ε_2 given in the second column of Table 2, we find that, for $\widetilde{\beta}_{\parallel h} = 1.0$, the following fitting parameters result:

$$\begin{aligned} c_1 &\cong -0.099 \\ c_2 &\cong 0.054 \\ \eta_{11} &\cong 1.18 \\ \eta_{22} &\cong 1.22 \end{aligned} \tag{13}$$

Note that, although equations (12a) and (12b) are explicitly independent of n_h/n_e, they are implicit functions of the relative hot proton density through the definition of $\beta_{\parallel h}$. So the result that both η_{11} and η_{22} are of order unity implies the physically plausible consequence that the maximum magnetic field energy density scales
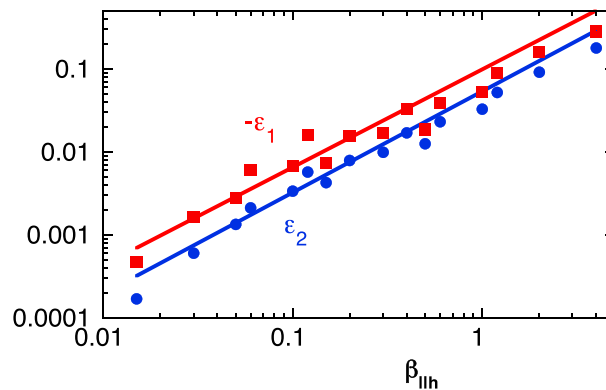
Figure 5. The fitting parameters $-\varepsilon_1$ (red points) and ε_2 (blue points) of the maximum fluctuating field energy densities from hybrid PIC simulations of the Alfvén-cyclotron instability at $\mathbf{k} \times \mathbf{B}_o = 0$ as functions of $\beta_{\parallel h}$. The individual symbols represent results from Table 2, whereas the solid lines represent the $\widetilde{\beta}_{\parallel h} = 1.0$ fits of equations (12a), (12b) and (13), that is, $-\varepsilon_1 = 0.099\beta_{\parallel h}{}^{1.18}$ and $\varepsilon_2 = 0.054\beta_{\parallel h}{}^{1.22}$.

approximately as the parallel thermal energy of the hot proton component. Figure 5 represents a broader range of results, including the 16 points of Table 2, showing that the parameter fits of equation (13) which were derived from the $\widetilde{\beta}_{\|h} = 1.0$ simulations are also approximately valid for values of that parameter ranging from 0.30 to 10.0.

The error analysis of these approximate fits to the simulated results is discussed in Appendix A. Table A3 shows that the fits to $\delta\mathbf{B}|_m^2/B_o^2$ become better as the relative density of the hot component increases. Combining this result with the error analyses from sections 2 and 3 leads us to the general conclusion that the larger the independent variables, the better the quality of the fit.

5. Conclusions

We have considered kinetic linear dispersion theory and hybrid PIC simulations of the Alfvén-cyclotron instability driven by a hot, anisotropic, tenuous proton component in the presence of a cool, isotropic, dense proton component in a magnetized, homogeneous, collisionless plasma. Linear theory yields scaling relations for the dimensionless maximum growth rate and the corresponding real frequency, whereas the simulations yield a scaling relation for the dimensionless magnetic field fluctuation energy density at instability saturation. All three scaling relations are relatively concise, analytic expressions which are functions of three independent dimensionless variables: n_h/n_e, $\beta_{\|h}$, and the hot proton temperature anisotropy. As each of these independent variables increases, so also increase the dependent variables, particularly the maximum growth rate and the maximum fluctuating fields. This is an expected result, because each independent variable contributes to the free energy driving the instability [e.g., *Min et al.*, 2016; *Fu et al.*, 2016]. Specifically, all three scaling relations are approximately linear functions of the temperature anisotropy [*Fu et al.*, 2016, Figures 3 and 6] on the range $2 \leq T_{\perp h}/T_{\|h} \leq 5$, but the dimensionless maximum growth rate is a considerably weaker function of n_h/n_e than the dimensionless fluctuating field energy density at saturation.

Our model of two bi-Maxwellian proton components is idealized; more realistic representations must eventually be used to more fully describe the complex plasma physics of actual magnetospheric ion dynamics. So future derivation of such scaling relations should include the presence of singly ionized helium [e.g., *Gendrin et al.*, 1984; *Chen et al.*, 2011; *Gary et al.*, 2012; *Fu et al.*, 2016] and other heavy ions [e.g., *Omidi et al.*, 2013], as well as the non-Maxwellian character [e.g., *Min et al.*, 2016] of many observed magnetospheric plasmas.

Appendix A

The accuracy of our fits to the scalings derived from linear dispersion theory can be estimated through use of

$$\Xi_\gamma \equiv \Sigma \left\{ \gamma_m/\Omega_p - \left[g_1 + g_2 \left(T_{\perp j}/T_{\|j} \right) \right] \right\}^2 / \left(\gamma_m/\Omega_p \right)^2$$

and

$$\Xi_\omega \equiv \Sigma \left\{ \omega_m/\Omega_p - \left[f_1 + f_2 \left(T_{\perp j}/T_{\|j} \right) \right] \right\}^2 / \left(\omega_m/\Omega_p \right)^2$$

where γ_m/Ω_p and ω_m/Ω_p are the exact growth rates and frequencies from the kinetic linear dispersion equation and g_1, g_2, f_1, and f_2 are the approximate values obtained by our fitting procedures. Similarly, estimates of the accuracy of our fits to the scalings derived from the hybrid simulations use

$$\Xi_\varepsilon \equiv \Sigma \left\{ \delta\mathbf{B}|_m^2/B_o^2 - \left[\varepsilon_1 + \varepsilon_2 \left(T_{\perp j}/T_{\|j} \right) \right] \right\}^2 / \left(\delta\mathbf{B}|_m^2/B_o^2 \right)$$

where $\delta\mathbf{B}|_m^2/B_o^2$ represents the dimensionless maximum fluctuating magnetic field energy density from a simulation and ε_1 and ε_2 are the approximate values obtained by our fitting procedures. Here Σ represents a sum over the several values of $T_{\perp j}/T_{\|j}$ in our computations as illustrated in Figures 1, 2, and 4 and $j = p$ for Figure 1 and $j = h$ for Figures 2 and 4. A 0 value of a Ξ variable represents exact agreement between the computed values and fitted variables, so that the goodness of fit decreases as this quantity increases.

For the case of a single bi-Maxwellian proton velocity distribution discussed in section 2 and illustrated in Figure 1, we obtain the linear theory results stated in Table A1.

Table A1. Error Analysis for the Linear Theory Results of the Case Illustrated in Figure 1

	$\beta_{\|p} = 0.05$	$\beta_{\|p} = 0.10$	$\beta_{\|p} = 0.25$	$\beta_{\|p} = 0.50$	$\beta_{\|p} = 1.0$	$\beta_{\|p} = 2.5$
Ξ_γ		5700	0.19	0.0094	0.0044	0.00026
Ξ_ω	0.0028	0.0011	0.00088	0.00077	0.00082	0.0036

The case of two proton components discussed in section 3 and illustrated in Figure 2 yields the linear theory results stated in Table A2.

Table A2. Error Analysis for the Linear Theory Results of the Case Illustrated in Figure 2

	$\beta_{\|h} = 0.05$	$\beta_{\|h} = 0.10$	$\beta_{\|h} = 0.25$	$\beta_{\|h} = 0.50$	$\beta_{\|h} = 1.0$
Ξ_γ	0.49	0.11	0.0050	0.0075	0.012
Ξ_ω		0.00032	0.00025	0.00014	0.00012

The case of two proton components discussed in section 4 and illustrated in Figure 4 yields the hybrid simulation results stated in Table A3.

Table A3. Error Analysis for the Hybrid PIC Simulation Results of the Case Illustrated in Figure 4

	$n_h/n_e = 0.05$	$n_h/n_e = 0.10$	$n_h/n_e = 0.20$	$n_h/n_e = 0.40$
Ξ_ϵ	1.75	0.27	0.062	0.018

We conclude that our fitting procedures yield improved agreement with theory and simulations with an increasing hot proton component β or an increasing n_h/n_e. Furthermore, our approximate analytic expressions do a better job of representing the real frequency than the maximum growth rate. Generally speaking, the relative accuracy of the scaling relations derived here increases with increasing values of the three independent variables, which should be a useful guideline in the application of these results.

References

Anderson, B. J., R. E. Erlandson, and L. J. Zanetti (1992), A statistical study of Pc 1-2 magnetic pulsations in the equatorial magnetosphere, 1. Equatorial occurrence distributions, *J. Geophys. Res.*, *97*(A3), 3075–3088, doi:10.1029/91JA02706.

Anderson, B. J., S. A. Fuselier, S. P. Gary, and R. E. Denton (1994), Magnetic spectral signatures in the Earth's magnetosheath and plasma depletion layer, *J. Geophys. Res.*, *99*, 5877–5892, doi:10.1029/93JA02827.

Bortnik, J., N. Omidi, L. Chen, R. M. Thorne, and R. B. Horne (2011), Saturation characteristic of electromagnetic ion cyclotron waves, *J. Geophys. Res.*, *116*, A09219, doi:10.1029/2011JA016638.

Chen, L., R. M. Thorne, and J. Bortnik (2011), The controlling effect of ion temperature on EMIC wave excitation and scattering, *Geophys. Res. Lett.*, *38*, L16109, doi:10.1029/2011GL048653.

Fraser, B. J., and T. S. Nguyen (2001), Is the plasmapause a preferred source region of electromagnetic ion cyclotron waves in the magnetosphere?, *J. Atmos. Sol. Terr. Phys.*, *63*(11), 1225, doi:10.1016/S1364-6826(00)00225-X.

Fu, X., M. M. Cowee, V. K. Jordanova, S. P. Gary, G. D. Reeves, and D. Winske (2016), Predicting electromagnetic ion cyclotron wave amplitude from unstable ring current plasma conditions, *J. Geophys. Res. Space Physics*, *121*, doi:10.1002/2016JA023303.

Gary, S. P. (1993), *Theory of Space Plasma Microinstabilities*, Cambridge Univ. Press, New York.

Gary, S. P., M. B. Moldwin, M. F. Thomson, D. Winske, and D. J. McComas (1994), Hot proton anisotropies and cool proton temperatures in the outer magnetosphere, *J. Geophys. Res.*, *99*, 23,603–23,615, doi:10.1029/94JA02069.

Gary, S. P., M. F. Thomsen, L. Yin, and D. Winske (1995), Electromagnetic proton cyclotron instability: Interactions with magnetospheric protons, *J. Geophys. Res.*, *100*, 21,961–21,972, doi:10.1029/95JA01403.

Gary, S. P., J. Wang, D. Winske, and S. A. Fuselier (1997), Proton temperature anisotropy upper bound, *J. Geophys. Res.*, *102*, 27,159–27,170, doi:10.1029/97JA01726.

Gary, S. P., K. Liu, and L. Chen (2012), Alfvén-cyclotron instability with singly ionized helium: Linear theory, *J. Geophys. Res.*, *117*, A08201, doi:10.1029/2012JA017740.

Gary, S. P., L. K. Jian, T. W. Broiles, M. L. Stevens, J. J. Podesta, and J. C. Kasper (2016), Ion driven instabilities in the solar wind: Wind observations of 19 March 2005, *J. Geophys. Res. Space Physics*, *121*, 30–41, doi:10.1002/2015JA021935.

Gendrin, R., M. Ashour-Abdalla, Y. Omura, and K. Quest (1984), Linear analysis of ion cyclotron interaction in a multicomponent plasma, *J. Geophys. Res.*, *89*, 9119–9124, doi:10.1029/JA089iA10p09119.

Jordanova, V. K., Y. Yu, J. T. Niehof, R. M. Skoug, G. D. Reeves, C. A. Kletzing, J. F. Fennell, and H. E. Spence (2014), Simulations of inner magnetospheric dynamics with an expanded RAM-SCB model and comparisons with Van Allen Probes observations, *Geophys. Res. Lett.*, *41*, 2687–2694, doi:10.1002/2014GL059533.

Liu, K., D. S. Lemons, D. Winske, and S. P. Gary (2010), Relativistic electron scattering by electromagnetic ion cyclotron fluctuations: Test particle simulations, *J. Geophys. Res.*, *115*, A04204, doi:10.1029/2009JA014807.

Meredith, N. P., R. M. Thorne, R. B. Horne, D. Summers, B. J. Fraser, and R. R. Anderson (2003), Statistical analysis of relativistic electron energies for cyclotron resonance with EMIC waves observed on CRRES, *J. Geophys. Res.*, *108*(A6), 1250, doi:10.1029/2002JA009700.

Min, K., J. Lee, K. Keika, and W. Li (2012), Global distribution of EMIC waves derived from THEMIS observations, *J. Geophys. Res.*, *117*, A05219, doi:10.1029/2012JA017515.

Min, K., K. Liu, and S. P. Gary (2016), Scalings of Alfvén-cyclotron and ion Bernstein instabilities on temperature anisotropy of a ring-like velocity distribution in the inner magnetosphere, *J. Geophys. Res. Space Physics*, *121*, 2185–2193, doi:10.1002/2015JA022134.

Omidi, N., J. Bortnik, R. Thorne, and L. Chen (2013), Impact of cold O^+ ions on the generation and evolution of EMIC waves, *J. Geophys. Res. Space Physics*, *118*, 434–445, doi:10.1029/2012JA018319.

Winske, D., and N. Omidi (1993), Hybrid codes: Methods and applications, in *Computer Space Plasma Physics: Simulation Techniques and Software*, edited by H. Matsumoto and Y. Omura, pp. 103, Terra Sci., Tokyo.

Zhang, J.-C., et al. (2014), Excitation of EMIC waves detected by the Van Allen Probes on 28 April 2013, *Geophys. Res. Lett.*, *41*, 4101–4108, doi:10.1002/2014GL060621.